

## Intra-tumoral Heterogeneity in Tumor Vasculature Correlates with ADC Quantification in Renal Masses

Qing Yuan<sup>1</sup>, Koji Sagiyama<sup>2</sup>, Yue Zhang<sup>1</sup>, Naira Muradyan<sup>3</sup>, Annanth Madhuranthakam<sup>1,2</sup>, Yin Xi<sup>1</sup>, Ivan E Dimitrov<sup>2,4</sup>, Vitaly Margulis<sup>5</sup>, James Brugarolas<sup>6,7</sup>, Payal Kapur<sup>5,8</sup>, and Ivan Pedrosa<sup>1,2</sup>

<sup>1</sup>Radiology, UT Southwestern Medical Center, Dallas, TX, United States, <sup>2</sup>Advanced Imaging Research Center, UT Southwestern Medical Center, Dallas, TX, United States, <sup>3</sup>iCAD, Inc., Nashua, NH, United States, <sup>4</sup>Philips Medical Systems, Cleveland, OH, United States, <sup>5</sup>Urology, UT Southwestern Medical Center, Dallas, TX, United States, <sup>6</sup>Internal Medicine, UT Southwestern Medical Center, Dallas, TX, United States, <sup>7</sup>Developmental Biology, UT Southwestern Medical Center, Dallas, TX, United States, <sup>8</sup>Pathology, UT Southwestern Medical Center, Dallas, TX, United States

**Target Audience:** Investigators interested in evaluation of tumor pathophysiology, particularly renal cell carcinoma (RCC), with DCE and DWI.

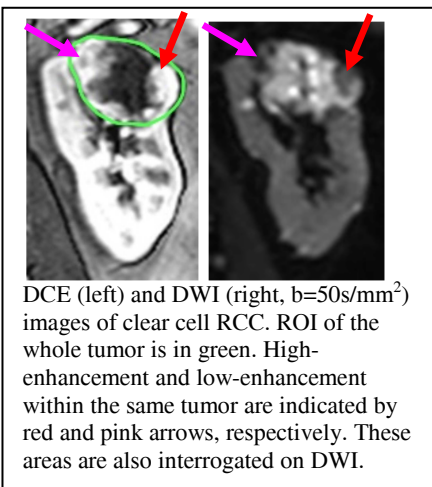
**Purpose:** Dynamic contrast-enhanced (DCE) MRI and diffusion-weighted imaging (DWI) have shown promise in characterization of renal masses. Pharmacokinetic DCE analysis evaluates tumor angiogenesis by quantifying tumor perfusion, permeability, vascularity, and extravascular extracellular space<sup>1</sup>. Apparent diffusion coefficient (ADC) calculated from DWI signal decay correlates with tumor cellularity in renal malignancies<sup>2</sup>. The biexponential intravoxel incoherent motion (IVIM) model allows for separation of pure tissue diffusion from pseudodiffusion due to capillary perfusion<sup>3</sup>. The purpose of this study was to investigate intra-tumoral heterogeneity of tumor perfusion-related quantitative measures and diffusion in renal masses *in vivo* and the potential correlation between these parameters.

**Methods:** This was a prospective, IRB-approved, HIPAA-compliant study. After signing an informed consent, patients scheduled for surgical resection of a renal mass were examined on a 3T dual-transmit MRI scanner with a 16-channel SENSE-XL-Torso coil (Achieva, Philips Medical Systems, Cleveland, OH). Coronal DWI of both kidneys was acquired using a respiratory-triggered (respiratory bellow or navigator) single-shot spin-echo echo-planar sequence with b-values of 0, 50, 100, 200, 450, 600, and 1000 s/mm<sup>2</sup>. For DCE MRI, a 3D spoiled gradient echo sequence was used to acquire coronal images of both kidneys with temporal resolution of 5 sec. To minimize respiratory motion during DCE imaging, three consecutive dynamic phases were obtained within each 15 sec breath-held acquisition period. A 15 sec period of free-breathing was allowed between consecutive acquisition periods. Three baseline dynamic phases were acquired, followed by administration of a bolus of 0.1 mmol/kg of gadobutrol (Gadavist; Bayer Healthcare Pharmaceuticals, Wayne, NJ) using a power injector at a rate of 2 cc/sec and a 20 cc saline flush at the same rate. The same MRI sequence was used to generate a T1 map (T1<sub>0</sub>) prior to contrast injection with three separate acquisitions with different flip angles (i.e. 10°, 5°, and 2°). DCE images were analyzed using the Tofts Model<sup>1</sup> after motion correction (iCAD, Inc., Nashua, NH). A population-averaged high-temporal-resolution arterial input function (AIF)<sup>4</sup> was used to quantify parametric maps of tumor vascular transfer constant (K<sup>trans</sup>), rate constant (k<sub>ep</sub>), blood plasma volume fraction (v<sub>p</sub>) and extravascular extracellular volume fraction (v<sub>e</sub>). The initial area under the concentration time curve integrated over the first minute (iAUC) was also computed. All parametric maps were exported as DICOM images to an Open-Source DICOM Viewer, OsiriX (v5.6, 64-bit). Region-of-interest analysis of the whole tumor (Whole), and areas with high- (High) and low-enhancement (Low) within the same tumor were manually drawn on DCE images (Figure) and then exported to parametric maps. Mean values of pharmacokinetic parameters in ROIs were tabulated. ROIs were manually drawn on diffusion images to match the ROIs on DCE images. ROI-based diffusion parameters were calculated using custom-written programs in MATLAB. A monoexponential model,  $S_i = S_0 * exp(-ADC * b_i)$ , was used to calculate ADC<sub>all</sub> using all b-values, and ADC<sub>slow</sub> using only the higher b-values (i.e. 450, 600, and 1000 s/mm<sup>2</sup>). An IVIM model,  $S_i = S_0 * (f_p * exp(-D_p * b_i) + (1 - f_p) * exp(-D_t * b_i))$ , was applied to compute pure tissue diffusion (D<sub>t</sub>), pseudodiffusion due to blood and tubular flow (D<sub>p</sub>), and pseudodiffusion fraction (f<sub>p</sub>) using all b-values. Linear mixed models were used for each variable to test the difference in the mean among different tumor regions, as well as the effects of diffusion model on ADC quantification. Rank based Friedman's tests were used for D<sub>p</sub> in order to cope with non-normal residuals (SAS 9.3).

**Results:** Twenty-one patients with 21 renal masses were included. Histopathologic diagnosis included 14 clear cell (9 low grade, 5 high grade) RCCs, 2 papillary RCCs, 1 chromophobe RCC, 3 oncocytomas, and 1 angiomyolipoma. Three patients with obvious respiratory motion artifacts on DWI were excluded. All DWI and DCE measures were statistically different among the three tumor regions as defined, except for D<sub>t</sub> and T1<sub>0</sub> (Table). The DCE-derived parameters K<sup>trans</sup>, k<sub>ep</sub>, v<sub>e</sub>, v<sub>p</sub>, and iAUC, as well as perfusion-related diffusion parameter D<sub>p</sub>, were significantly higher in areas with high-enhancement compared to low-enhancing regions, indicative of increased tumor angiogenesis in these regions. Conversely, ADC values in high-enhancement tumor regions were lower, indicating significantly slower water diffusion due to higher cellularity, compared to low-enhancement tumor regions. ADC values estimated from monoexponential model using all b values are significantly higher than ADC values calculated from monoexponential model using higher b-values and IVIM model. No significant difference was found between ADC values calculated from monoexponential model using higher b-values and IVIM model.

**Discussion:** DCE and DWI allow for assessment of intra-tumoral heterogeneity in tumor vascularity and cellularity in renal masses. Areas with increased vascularity demonstrate lower ADC values suggesting increased cellularity in areas with increased angiogenesis. IVIM diffusion parameters provide true tissue diffusion estimates as well as potential perfusion information. However, biexponential fitting requires DWI acquisition of multiple b-values with longer scan time, which is prone to motion artifacts in the abdomen. As a result, tissue diffusion D<sub>t</sub> from IVIM model was less reliable compared with ADC determinations from high b-values (ADC<sub>slow</sub>).

**Conclusion:** Our study demonstrates that DCE and DWI can be utilized to detect intra-tumoral heterogeneity in angiogenesis and water diffusion in renal masses. Differences in tissue diffusion between high and low perfusion tumor regions suggests that angiogenesis correlates with heterogeneity in tumor cellularity. Future pathologic tissue analysis will be performed to confirm the MRI findings.



Mean values of DWI and DCE measures of whole tumor, high and low enhancement areas. P values < 0.05 are statistically significant.

	Whole	High	Low	High vs. Low
ADC <sub>all</sub> (mm <sup>2</sup> /s)	1.90	1.66	2.05	<.0001
ADC <sub>slow</sub> (mm <sup>2</sup> /s)	1.43	1.17	1.59	0.0002
D <sub>t</sub> (mm <sup>2</sup> /s)	1.32	1.26	1.40	0.6916
D <sub>p</sub> (mm <sup>2</sup> /s)	75.06	188.64	87.96	0.043
f <sub>p</sub>	0.31	0.27	0.42	0.0446
K <sup>trans</sup> (min <sup>-1</sup> )	0.92	2.06	0.35	<.0001
k <sub>ep</sub> (min <sup>-1</sup> )	2.03	3.78	1.39	<.0001
v <sub>e</sub>	0.44	0.54	0.31	<.0001
v <sub>p</sub>	0.03	0.05	0.01	0.0068
iAUC (mM*sec)	36.17	53.10	18.41	0.0005
T1 <sub>0</sub> (sec)	1.87	1.98	2.01	0.9667

**References:** 1. Tofts PS, et al, JMRI 10:223-232 (1999); 2. Manenti G et al, Radiol Med 113:199-213 (2008); 3. Le Bihan, et al, Radiology 161:401-407 (1986); 4. Parker GJM, et al, MRM 56:993-1000 (2006).

**Acknowledgement:** This study is supported by the grant NIH/NCI 1R01CA154475-01.